Additive Manufacturing 22 (2018) 146–152

Contents lists available at ScienceDirect

Additive Manufacturing

journal homepage: www.elsevier.com/locate/addma

Computed tomography metrological examination of additive manufactured acetabular hip prosthesis cups

Nadia Kourra[a,*], Jason M. Warnett[a], Alex Attridge[a], Greg Dibling[b], James McLoughlin[b], Sarah Muirhead-Allwood[c], Richard King[d], Mark A. Williams[a]

[a] IMC, WMG, University of Warwick, CV4 7AL, UK
[b] Corin Ltd., Corinium Centre, Cirencester, Gloucestershire GL7 1YJ, UK
[c] London Hip Unit 4th Floor, 30 Devonshire Street, London W1G 6PU, UK
[d] University Hospitals Coventry and Warwickshire, Clifford Bridge Road, Coventry CV2 2DX, UK

ARTICLE INFO

Keywords:
Computed tomography
Additive manufacturing
Image processing
Non-destructive testing
Metrological application
Local thickness analysis
Hip prosthesis
Bone ingrowth

ABSTRACT

Additive manufacturing (AM) is uniquely suitable for healthcare applications due to its design flexibility and cost effectiveness for creating complex geometries. Successful arthroplasty requires integration of the prosthetic implant with the bone to replace the damaged joint. Bone-mimetic biomaterials are utilised due to their mechanical properties and porous structure that allows bone ingrowth and implant fixation. The predictability of predetermined interconnected porous structures produced by AM ensures the required shape, size and properties that are suitable for tissue ingrowth and prevention of the implant loosening. The quality of the manufacturing process needs to be established before the utilisation of the parts in healthcare. This paper demonstrates a novel examination method of acetabular hip prosthesis cups based on X-ray computed tomography (CT) and image processing. The method was developed based on an innovative hip prosthesis acetabular cup prototype with a prescribed non-uniform lattice structure forming struts over the surface, with the interconnected porosity encouraging bone adhesion. This non-destructive, non-contact examination method can provide information of the interconnectivity of the porous structure, the standard deviation of the size of the pores and struts, the local thickness of the lattice structure in its size and spatial distribution. In particular, this leads to easier identification of weak regions that could inhibit a successful bond with the bone.

1. Introduction

According to ASTM standard terminology [1], additive manufacturing (AM) is defined as "the process of joining materials to make objects from 3D model data, usually layer upon layer, as opposed to subtractive manufacturing methodologies, such as traditional machining". The continuing fast development of AM in the last four decades demonstrates the advantages of the technology. The reduction or even elimination of fixturing, cutting tools and minimal post processing, improves the product development cycle time. AM is the only manufacturing process that allows the build of complex geometries to reduce assembly requirements, increase the functionality of the product, and improve their energy footprint [2–4]. According to Gao et al. [5] the unique capabilities of AM include design flexibility, cost effective geometric complexity, assembly free designs, time and cost efficiency in production run for low part quantities. Due to the wide application spectrum of AM, it receives great interest from niche markets such as aerospace, medicine and biological systems [2,3]. In particular the application of AM for healthcare/medical customised products based on the requirements of the patient is expected to improve population wellbeing [3].

The application of AM in the healthcare industry is relatively new with the first applications surfacing approximately a decade ago [6]. These applications are established with numerous examples in maxillofacial prosthesis, dentistry, surgical guides and orthopaedic implants such as total hip prosthesis [6–14]. AM can produce customised products based on the patients requirements and shape personalised healthcare with bespoke surgical implants and assistive devices such as surgical guides [3,10,15]. Also surgical teams can utilise 3D imaging methods, AM models and surgical guides to establish surgical plans to minimise any complications by using hardwearing, corrosion resistant metals with precise design that ensures sufficient rigidity [10,15].

Arthroplasty, such as hip and knee replacement, is a surgical procedure that improves the functionality of joints. The demand for such surgical procedures is high and allows the patients to move with reduced pain and have more active lifestyle. A successful joint surgery

* Corresponding author.
E-mail address: N.Kourra@warwick.ac.uk (N. Kourra).

https://doi.org/10.1016/j.addma.2018.04.033
Received 23 November 2017; Received in revised form 20 February 2018; Accepted 26 April 2018
Available online 02 May 2018

should be painless, stable and provide freedom of movement with an acceptable service lifespan [16]. One of the main complications of arthroplasty is the loosening of the prosthesis from the bone [13,17], bone-mimetic biomaterials are utilised to achieve better bone ingrowth and implant fixation. The most common manufacturing techniques to produce the required porous metals appropriate for such applications are space holder technology and AM [18].

The main advantage of AM over other manufacturing techniques for the production of interconnected lattice structures is the greater predictability of the manufactured product. The controlled shape and size of the interconnected structure ensure the biomimetic characteristics that will enable tissue ingrowth and prevent the prosthesis loosening [18,19]. However, the success of the parts depends on the achieved quality and therefore the manufacturing process needs to be examined and tested. Conventional tests include destructive examinations that provide limited data and potentially destroy problematic areas.

This paper demonstrates a novel examination method of AM acetabular hip prosthesis cups based on X-ray computed tomography (CT) and image processing. The development of this non-destructive, non-contact examination was based on the inspection of a new prototype. The results provide information of the interconnectivity of the lattice structure, through evaluation of segmented pores and struts. The analysis demonstrates the local thickness of the structure in histograms and visually represent the results for easier identification of weak areas. The specimen discussed in this paper is a prototype used to develop and test the method and does not provide any conclusions on the quality of the manufacturing method, process, design of the components and material selection.

2. Computed tomography

X-ray computed tomography (CT) is well known for its medical application and in recent years, it has been applied to non-destructive industrial quality examinations. The industrial application of this technology has developed due to the growing need to examine the quality of complex engineering components such as AM parts [20]. The reconstructed 3D model produced by CT scanning demonstrates outer and inner geometries as well density fluctuations. This technology is applied in numerous industrial applications for the examination and certification of different manufacturing procedures and materials [21] as a non-destructive test (NDT).

The layout of a typical lab-based cone-beam X-ray CT machine is provided in Fig. 1. X-ray CT collects a series of radiographs through a 360-degree rotation of the work-piece that are then reconstructed to create a 3D model of the examined object. The produced X-rays need to have sufficient energy to penetrate the examined object and travel to the detector where the radiographs are collected [22]. In a well-calibrated CT system, the quality of the radiographs depends on the characteristics of the X-rays, the settings of the detector and the exposure time per radiograph. Each pixel of a radiograph has a grey value that equates to the proportion of X-rays that have not been absorbed by the work-piece [23,24]. After the completion of the scan, the radiographs are reconstructed with Filtered Back Projection (FBP) algorithm that transforms the radiographs to a 3D representation of the object. The algorithm produces 2D slices through the object, which as a stack represent the object as a collection of 3D pixels, called voxels [25]. Each voxel has an associated grey value that represents the atomic density of the material; air has the lowest grey value (black) while materials with high atomic number are assigned a higher grey value (white). The 3D data can be analysed further to provide dimensional information, volumetric analysis and other quantification [26].

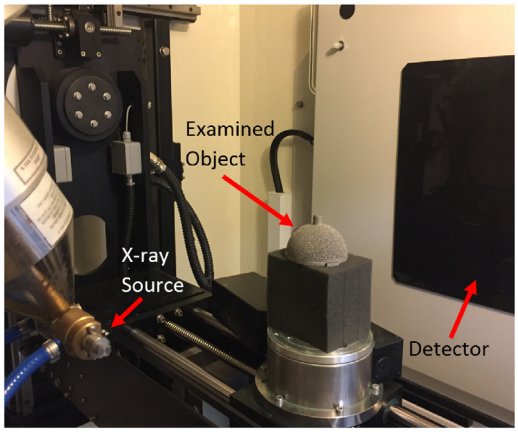

Fig. 1. Computed tomography (CT) lay out, with the source at left side, the examined object on the manipulator and the detector at the right side of the image.

Numerous studies discuss the uncertainty related to CT scanning [27–30]. This may be influenced by many factors such as image noise, pixel size, geometric hardware calibration and the selected magnification. In order to obtain dimensional measurements from CT, a specific procedure has to be followed. The measurements are taken based on a threshold selection, typically Otsu [31] based on class separation, that separates the material from air based on the grey value of voxels. Due to the uncertainty related to the threshold selection, a calibrated part needs to be scanned prior and post scanning or together with the examined object. The calibrated part has features that can provide threshold independent measurements such as holes or spheres. The CT measurements can then be updated according to these known measurements of the calibrated part by voxel rescaling. This procedure follows VDI/VDE 2630 Part 1.2 and it has been shown to reduce the measurements errors from 2% to as low as 0.2% for single material scans [32,33].

CT scanning can provide non-destructive, non-contact examination as well as dimensional measurements of complex engineering components. One of the main reasons for the rise of AM is due to its capabilities to produce complex engineering components. This become an issue in itself as no other NDT methods can provide the required examination to appraise sufficiently their suitability. Therefore, CT is the only holistic examination available to provide qualitatively and quantitatively the required information without destroying any components. The application of this technology is considerably new as an NDT and in dimensional metrology, nevertheless recent studies on Real Time Tomography (RTT) X-ray CT demonstrate its potential in production examinations [34]. As a result, international standard organisations have not yet provided any standards that can be followed to ensure the quality of the examinations, although they are currently being developed such as ISO/NP 10360-11 [35]. In order to overcome these limitations, CT guidelines provided from organisations such as VDI/VDE [32] have to be followed. Here, it is suggested that the same scanning settings are used when multiple parts of the same design are examined for comparability purposes.

3. Methodology

The material of the examined AM acetabular hip prosthesis cup is Ti6Al4V. It was produced by Electron Beam Melting (EBM) method and Arcam EBM Q10 (A GE Additive Company) that is often used for the production of orthopaedic implants. Fig. 2 shows the prosthesis and demonstrates its non-uniform lattice structure. The method presented here was developed to examine quantitatively the interconnectivity of the lattice structure of the acetabular hip prosthesis produced by AM to ensure optimum bone ingrowth and implant fixation. The main objectives of the method are to non-destructively examine the components for quality insurance, identify cracks or internal porosity in the main body and ensure that the porous structure has the expected characteristics. The non-uniform lattice structure can be separated as material, named struts, and the pores. CT scanning collected the 3D data and

Fig. 2. The geometry of the examined AM acetabular hip prosthesis cup is hemispherical and the lattice structure that ensures optimum bone ingrowth is non-unidormal.

image processing enabled dimensional measurements. All of the technologies and software packages used in this method are provided in Table 1. The method was developed on a prototype acetabular prosthesis and the results provided in the next section are not representative to the manufacturing method, process, design of the parts and material selection.

3.1. CT scanning

The examined prototype of the acetabular cup was scanned at a 43 µm voxel resolution with the optimum scanning settings provided in Table 2. The achieved resolution is the best possible resolution based on the size of the specimen. The CT scanning settings were chosen to provide sufficient penetration and minimise noise based on the achieved grey values. The entire specimen remains in view during all of the projections while a physical filter was used to reduce beam hardening effects and cupping artefacts. This was further adjusted through pre-processing projections using a beam hardening reduction algorithm with a standard second order polynomial correction filter [36].

In CT scanning the threshold selection to separate material and background affects dimensional measurements as boundaries of objects experience partial volume and unsharpness effects, intrinsic to the scanning process, in addition to error in the voxel size due to geometric calibration of the hardware. By taking measurements using traceable metrological equipment such as a Coordinate Measuring Machine (CMM), the voxel size can be scaled according to these measurements to compensate for these errors. The voxel rescaling method used in this investigation follows the VDI/VDE 2630 Part 1.2 guidelines shown to reduce the measurement uncertainty [32].

The scan of the examined object was performed with a calibrated work-piece with known threshold independent measurements that are then used to update the voxel size of the scanned data. The part was calibrated with traceable tactile CMM, which provided three centre-to-centre measurements. The measurements were obtained in a controlled environment with a standard temperature of 20 °C, the repeatability of the tactile measurements is 1 µm verified according to ISO 3650:1999 [37] and the uncertainty is 3 µm according to ISO 10360-8:2013 [38]. The scan data of the calibrated work-piece identified the same three centre to centre measurements, Fig. 3, and the voxel size was rescaled in VG Studio Max according to CMM measurements to represent the known three centre to centre measurements. After the voxel rescaling procedure, the measurements were repeated and the maximum measured error of the calibrated artefact was smaller than 0.2 voxel size.

Table 1
Machines and software used in this method.

Machines &Software used	Name	Producer	Year
X-ray CT scanner	X-TEK XT H 225/320 LC	Nikon Metrology, UK	
Optical CMM scanner	NEXIV VMA 4540	Nikon Metrology, UK	
CT Reconstruction software	CT Pro 2.4	Nikon Metrology, UK	2016
CT Inspection software	VG Studio Max 2.2	Volume Graphics GmbH, Germany	2016
Analysis Software	Matlab 2016b	MathWorks, USA	2017
	ImageJ 1.51k	Wayne Rasband	2017
	Avizo 9.0.2	FEI Visualisation Sciences Group	2017

Table 2
CT scanning settings.

CT scanning settings	
Voltage (kV)	215
Power (W)	33
Exposure time (s)	2.8
Gain (dB)	24
Voxel size (µm)	43
Filter (mm Sn)	2

3.2. Image processing

The aligned and voxel corrected data were exported in DICOM[1] image format and imported for automated image processing in MATLAB (MathWorks, 2017). The acetabular cup is hemispherical in shape, thus the resultant image stack from the CT scan that is to be analysed, consist of concentric circles with the outer periphery formed of the struts (Fig. 4). The pixel size in a single image is equal to the voxel size of the scan setup, with the image taken to be one voxel thick.

The centre of the hemisphere taken at the base of the struts was identified based on 36 thresholded points from various points of the examined specimen. Hough transform is used to identify the circle and its centre in each image and this information is used to identify the position and centre of the hemisphere with the MATLAB function `ellipsoid_fit` (Petrov, 2015).[2] The information provided by this function, the centre and radius of the hemisphere, are then utilised to separate the porous structure from the main body. The separation of the maximum circle that includes the full length of the struts, from the rest of the volume is achieved by calculating the maximum radius initiating from the already identified circle. The maximum radius is then used to

[1] Digital Imaging and Communications in Medicine (DICOM).

[2] Function available in MATLAB's file exchange website by Yury Petrov, Oculus VR, September 2015.

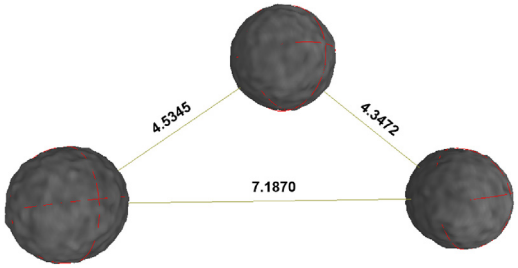

Fig. 3. Recalibration of the voxel size is achieved through known measurements of calibrated specimen. The measurements are in mm.

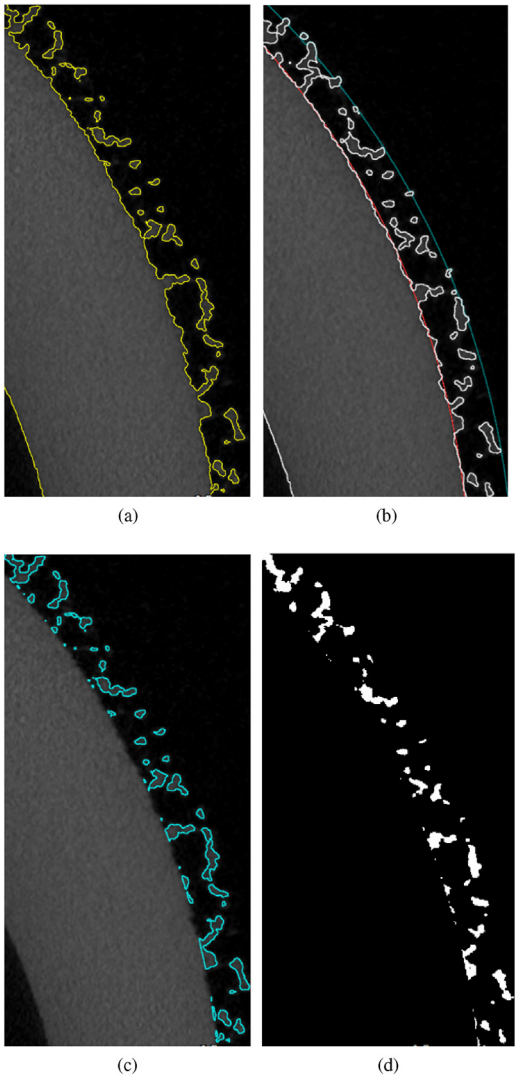

Fig. 4. The stages of segmentation: (a) thresholding material, (b) identification of inner and outer boundaries of struts and pores, (c) segmentation and (d) binarisation of images. The images are provided as demonstration of the method and they were created with VG studio Max.

separate the background from the porous structure. The specific acetabular cup provided includes protrusions that is not relevant to the characterisation to the porous structure and those areas are removed from the 3D matrix based on their geometry.

The class separation method of Otsu thresholding [31] was applied to the grey scale data, suitable for single material scans. The data was separated and exported into two groups of images; a set for the struts investigation and a set for the pores investigation.

The images were imported into ImageJ and the 3D local thickness analysis tool was used as in Fig. 5, where the distance in every direction of each pixel to the closest material boundary is calculated. The local thickness images were evaluated in MATLAB (MathWorks, 2017). All of the pixels are examined to identify the minimum and maximum values, calculate the average and the standard deviation of the local thickness analysis. A global view of the distribution can be seen by viewing the values as a histogram. The tolerance limits of thickness were selected based on the work of Taniguchi et al. [19] as an example of typical manufacturing tolerances.

The local thickness evaluation was examined in 3D using Avizo (FEI Visualisation Sciences Group, 2017) where the struts region are represented with different colours based on the local thickness analysis results. The pore region was separated into regions with the function separate objects. This is based on the calculated distance map and the interconnectivity of the regions, which is then used to create a medial axis to mask the distance map. The separation of the pores is strictly affected by the contrast of the local maxima and minima of the distance map. The sub-regions are separated based on their sizes and colour coded based on the mean and maximum values. Further statistical analysis is performed to provide local thickness maxima and minima of the data as qualitative images to demonstrate the potentially weak areas.

4. Results

This method provides quantitative and qualitative results, with statistical analysis and visual representations of local thickness for the entire structure. The results are divided into the local thickness of the struts and then the pores. The maxima, minima as well as the mean of the local thickness are identified for every point. The results provide a full characterisation of the struts and the porous structure. CT scanning can identify internal porosity and cracks in the main body of these specimens but is omitted in the analysis that follows.

The results of the statistical analysis provided by this method can be found in Table 3 and can be utilised for comparisons between different parts. The original voxel size was 43.004 μm and the achieved voxel size after rescaling was 43.875 μm. Table 3 also provides information about the maximum, mean, minimum and standard deviation of local thickness values of pores and struts. The maximum pores value is 1034.9 μm and the mean pore value is 457.92 μm, while the standard deviation is 163.21. The maximum struts value is 568.87 μm and the mean struts value is 261.19 μm, while the standard deviation is 87.02. The minimum value for both pores and struts is 87.75 μm demonstrating the limitation of this method since it is twice the rescaled voxel size and the smallest identifiable local thickness value.

The volume fraction of pores and struts can be used as quantitative comparisons for quality assurance. The percentages of the local thickness of pores and struts can ensure the suitability of the acetabular cup prosthesis, since research shows that porous structures of 600 μm provide optimum implant fixation [19]. In this paper the selection of lower and upper specification limits were 225 μm and 1158 μm, 173 μm and 811 μm for pores and struts respectively. These limits were selected based on the mean and standard deviation of the work of Taniguchi et al. [19], as an example to demonstrate the capabilities of the method. The results demonstrate that 14.55% of porous structure has a porous structure smaller than 225 μm. No pores were detected to have sizes close to the upper specification limit. The 85.45% of porous structure has sizes that allow sufficient implant fixation. Similarly, due to the required size of the porous structure the tolerances of the struts structure are between 173 μm and 811 μm to ensure structural stability while allowing bone ingrowth. The 17.96% of the struts structure is smaller than 173 μm and no struts were detected to have sizes more than 600 μm, consequently, the 82.04% of struts structure provides sufficient stability. Fig. 6 demonstrates the number of occurrences of local thickness in histograms for Fig. 6a pores and Fig. 6b struts providing

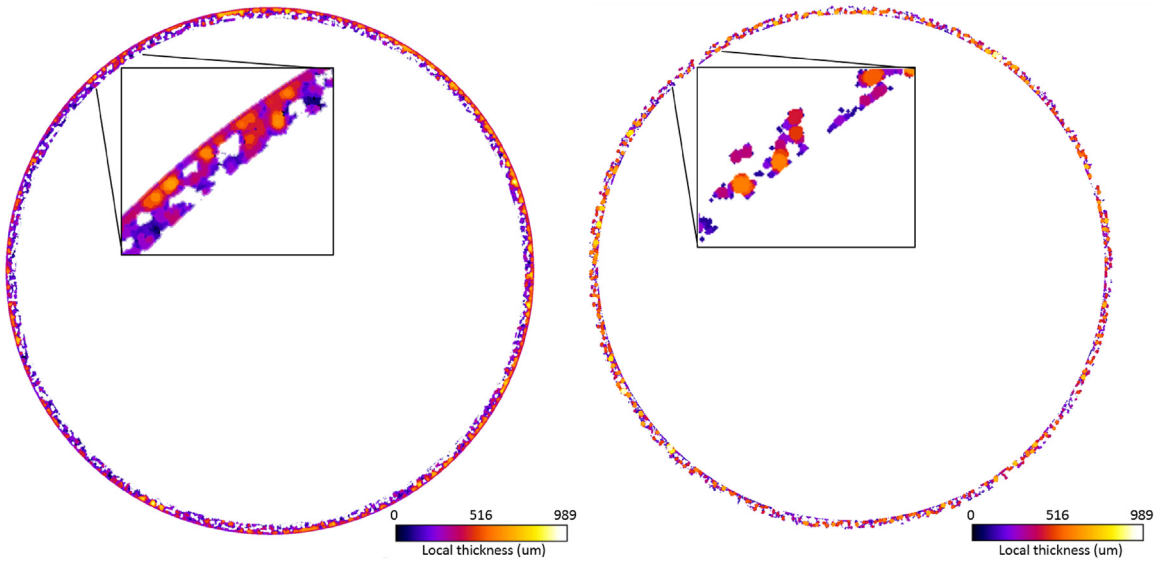

(a) (b)

Fig. 5. The local thickness analysis performed in ImageJ. The different diameter spheres fitted are demonstrated in different colours for (a) pores and (b) struts.

Table 3
Pores and struts statistics for the established voxel size. The size limits shown in percentages are selected based on Taniguchi et al. [19].

Measurements (μm)	
Original voxel size	43.004
Rescaled voxel size	43.875
Pores	± 3 μm
Maximum (μm)	1034.9
Mean (μm)	457.92
Minimum (μm)	87.75
Standard deviation	163.21
% < 225 (μm)	14.55
% > 1158 (μm)	0
Struts	± 3 μm
Maximum (μm)	568.87
Mean (μm)	261.19
Minimum (μm)	87.75
Standard deviation	90.19
% < 173 (μm)	17.96
% > 811 (μm)	0

statistical information that can highlight quality issues. The statistical results can be used for comparisons when a series of components are examined. Further examination of the pores and struts structure can be found in the cumulative frequency graphs in Fig. 7. These graphs demonstrate the percentage of pores at each size. Fig. 7a shows that > 70% of the pores has sizes < 600 μm, while the subsequent 10% reaches sizes of 650 μm. Only 0.2% of pores had thickness > 900 μm. Fig. 7b shows that 60% of the struts has dimension < 300 μm, while 25% are smaller than 200 μm. Finally, only 0.3% of struts have local thickness > 500 μm.

The image processing analysis also provides the examination of the results in volumetric representation. Fig. 8 visually represents the local thickness results overlaid on the acetabular cup for the easy identification of weak areas. Fig. 8a and b show the local thickness results in different colours while Fig. 8c and d display the location of local thickness maxima and mean. These representations can assist in the identification of problematic areas in a systematic production study that examines all or a fraction of the produced parts.

CT scanning can also provide useful information on other defects related to AM acetabular hip prosthesis such as cracks and porosity in

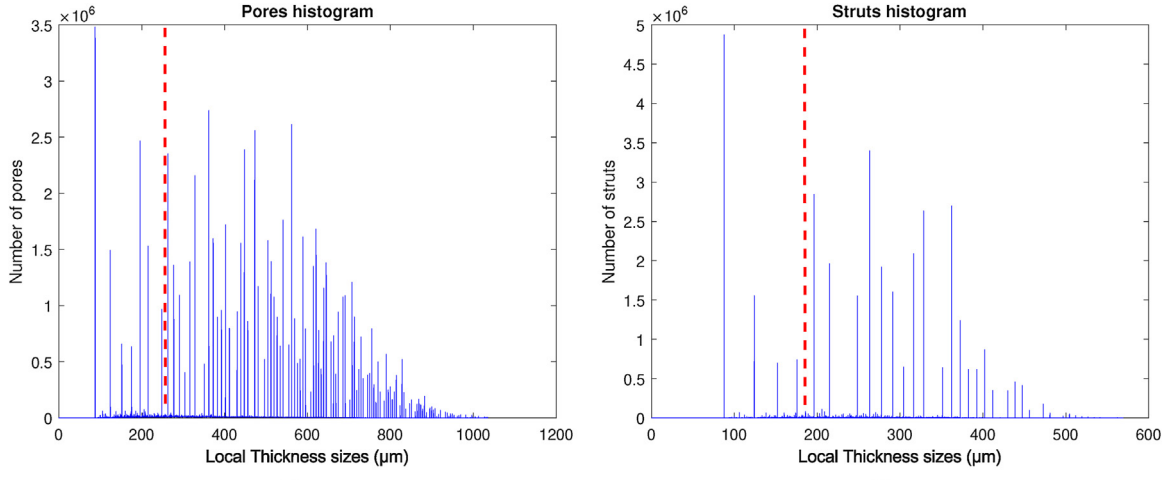

(a) (b)

Fig. 6. The number of occurrences of each pore and strut size are presented in histograms, (a) pores and (b) struts. The lower selected limit is shown in the red dotted line. (For interpretation of the references to color in this figure legend, the reader is referred to the web version of this article.)

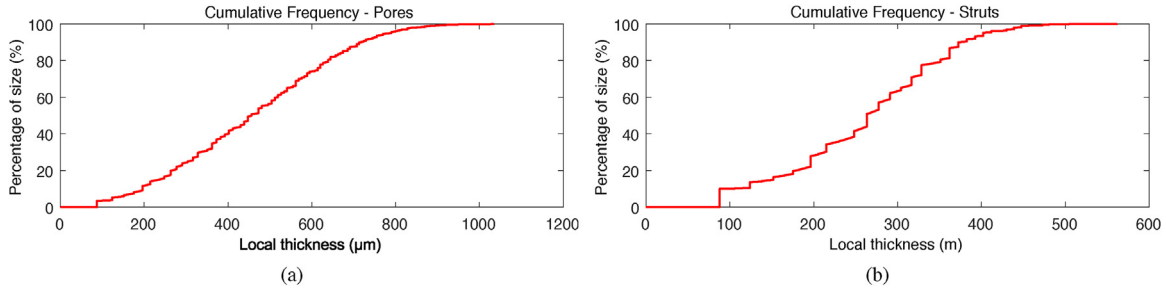

(a) (b)

Fig. 7. Cumulative frequency of (a) pores and (b) struts demonstrate the percentage of size for the different achieved local thickness.

the main body of the part, as well as powder trapped within the porous structure. These defects can be identified during the preparation of image processing. The method described in this paper concentrates on the porous structure of AM acetabular hip prosthesis with image processing. It provides accurate dimensional measurements by reducing human interference and error while following metrological guidelines [32].

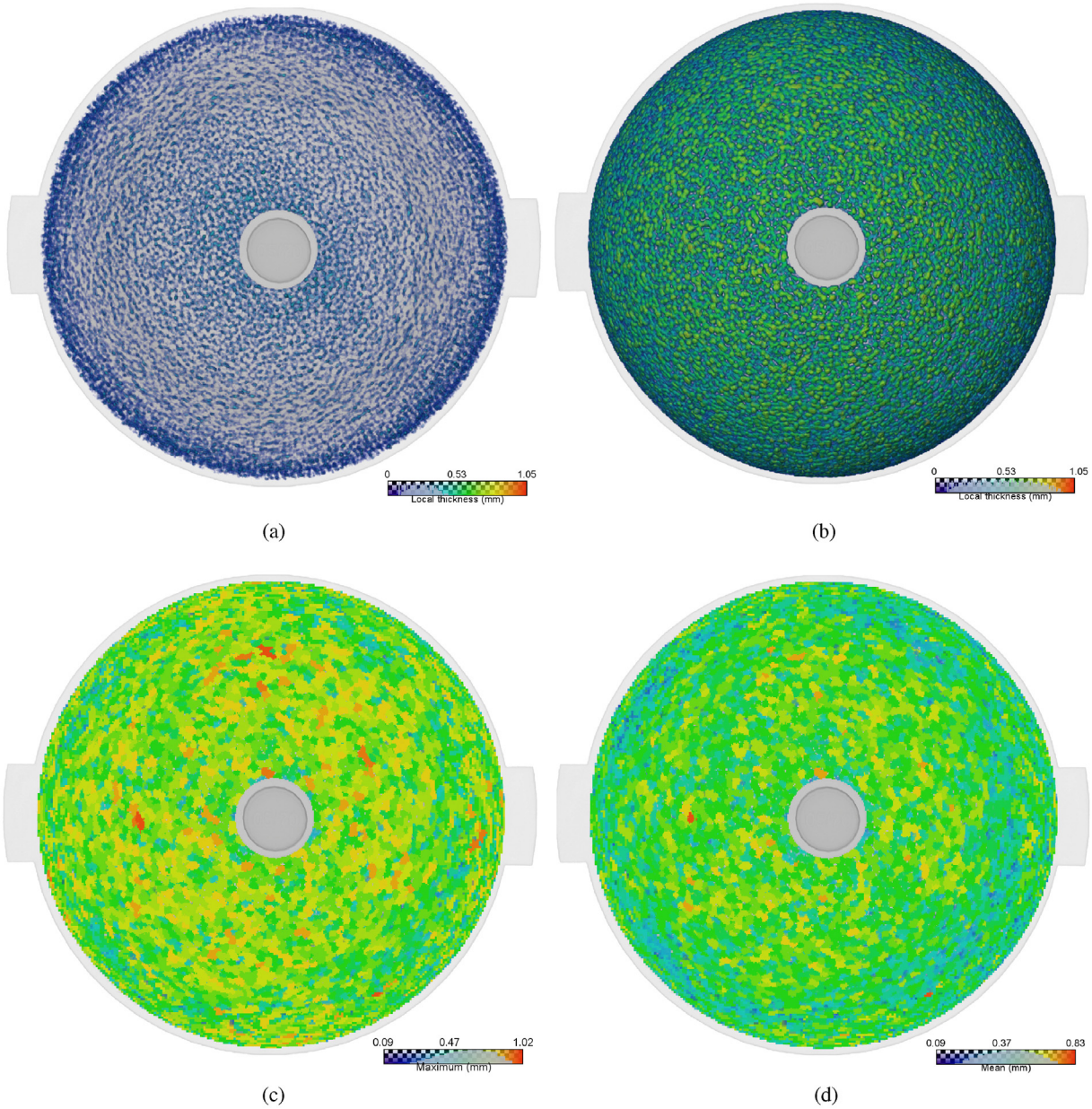

(a) (b) (c) (d)

Fig. 8. The results of the image processing analysis are demonstrated in 3D models for the better understanding of the issues and their location, (a) and (b) demonstrate the local thickness per pixel in different colours for struts and pores respectively for the same specimen, (c) shows the maximum and (d) the mean values of the local thickness at each point of the pore analysis.

5. Conclusions

This paper demonstrates the application of CT scanning for the non-destructive examination of complex AM parts that cannot be examined sufficiently with any other method. The novel method presented here, it examines a prototype of acetabulum hip prosthesis and provides quantitative and qualitative results through image processing. This method was developed to provide quality inspection and characterisation of the porous structure that affects the implants fixation. The results provided in this paper are not representative of the manufacturing method, process, design of the part and material selection.

The method utilises CT scanning to collect the required to data and image analysis to provide quantitative and qualitative results. The results can be separated in statistical analysis and volumetric representations to ease the examination. The method utilised CT software, MATLAB and ImageJ, with the majority of the image processing is automated to minimise human error. The volumetric representation of the results demonstrates the statistical analysis holistically so they can be examined visually. The results presented demonstrate the capabilities of the method and further statistical calculations and analysis are available if they are required.

Future scans should be scanned and reconstructed with the same settings for consistency. The accuracy of the analysis was ensured through several repetitions, however, further statistical analysis is planned to ensure the accuracy of the CT scanning. This method will be used as a quality examination of a new AM process and different software will be tested and evaluated to minimise computation times. Future planned work includes the comparison of different destructive and non-destructive methods to ensure the accuracy of this method in the examination of the surface roughness of the internal struts. Much progress has already been made in this area using CT as per Thompson et al. [39], which could be suitably exploited in this application.

Acknowledgements

The authors would like to thank Corin Ltd for providing the materials for this method and EPSRC for funding this project.

References

[1] ASTM, F2792-10e1 Standard Terminology for Additive Manufacturing Technologies, ASTM International, 2010.
[2] B. Vayre, F. Vignat, F. Villeneuve, Metallic additive manufacturing: state-of-the-art review and prospects, Mech. Ind. 13 (2) (2012) 89–96.
[3] S. Huang, P. Liu, A. Mokasdar, L. Hou, Additive manufacturing and its societal impact: a literature review, Int. J. Adv. Manuf. Technol. 67 (5–8) (2013) 1191–1203.
[4] H. Bikas, P. Stavropoulos, G. Chryssolouris, Additive manufacturing methods and modelling approaches: a critical review, Int. J. Adv. Manuf. Technol. 83 (1–4) (2016) 389–405.
[5] W. Gao, Y. Zhang, D. Ramanujan, K. Ramani, Y. Chen, C.B. Williams, C.C.L. Wang, Y.C. Shin, S. Zhang, P.D. Zavattieri, The status, challenges, and future of additive manufacturing in engineering, Comput. Aided Des. 69 (2015) 65–89.
[6] P. Liacouras, J. Garnes, J. Roman, A. Petrich, G.T. Grant, Designing and manufacturing an auricular prosthesis using computed tomography, 3-dimensional photographic imaging, and additive manufacturing: a clinical report, J. Prosthet. Dent. 105 (2) (2011) 78–82.
[7] L.E. Murr, S.M. Gaytan, E. Martinez, F. Medina, R. Wicker, Next generation orthopaedic implants by additive manufacturing using electron beam melting, Int. J. Biomater. (2012) 2012.
[8] M. Salmi, K.S. Paloheimo, J. Tuomi, T. Ingman, A. Makitie, A digital process for additive manufacturing of occlusal splints: a clinical pilot study, J. R. Soc. Interface 10 (84) (2013) 20130203.
[9] M. Salmi, J. Tuomi, K.S. Paloheimo, R. Bjorkstrand, M. Paloheimo, J. Salo, R. Kontio, K. Masimaki, A.A. Makitie, Patient specific reconstruction with 3D modelling and DMLS additive manufacturing, Rapid Prototyping J. 18 (3) (2012) 209–214.
[10] R. Bibb, D. Eggbeer, P. Evans, A. Bocca, A. Sugar, Rapid manufacture of custom fitting surgical guides, Rapid Prototyping J. 15 (5) (2009) 346–354.
[11] N. Al Maortadi, Q. Jones, D. Eggbeer, J. Lewis, R.J. Williams, Fabrication of a resin appliance with alloy components using digital technology without an analogue impression, Am. J. Orthod. Dentofac. Orthop. 148 (5) (2015) 862–867.
[12] D. Eggbeer, R. Bibb, P. Evans, L. Ji, Evaluation of direct and indirect additive manufacture of maxillofacial prostheses, Proc. Inst. Mech. Eng., Part H J. Eng. Med. 226 (9) (2012) 718–728.
[13] S. Rahmati, F. Abbaszadeh, F. Farahmand, An improved methodology for design of custom made hip prostheses to be fabricated using additive manufacturing technologies, Rapid Prototyping J. 18 (5) (2012) 389–400.
[14] A. Thompson, D. McNally, I. Maskery, R.K. Leach, X-ray computed tomography and additive manufacturing in medicine: a review, Int. J. Metrol. Qual. Eng. 8 (17) (2017).
[15] S. Peel, D. Eggbeer, "Additively manufactured maxillofacial implants and guides " achieving routine use, Rapid Prototyping J. 22 (1) (2016) 189–199.
[16] A. Rabiei, Recent developments and the future of bone mimicking: materials for use in biomedical implants, Expert Rev. Med. Devices 7 (6) (2010) 727–729.
[17] M. Cronskar, M. Backstrom, L.E. Rannar, "Production of customized hip stem prostheses" a comparison between conventional machining and electron beam melting (EBM), Rapid Prototyping J. 19 (5) (2013) 365–372.
[18] G. Campoli, M.S. Borleffs, S.A. Yavari, R. Wauthle, H. Weinans, A.A. Zadpoor, Mechanical properties of open-cell metallic biomaterials manufactured using additive manufacturing, Mater. Des. 49 (2013) 957–965.
[19] N. Taniguchi, S. Fujibayashi, M. Takemoto, K. Sasaki, B. Otsuki, T. Nakamura, T. Matsushita, T. Kokubo, S. Matsuda, Effect of pore size on bone ingrowth into porous titanium implants fabricated by additive manufacturing: an in vivo experiment, Mater. Sci. Eng. 59 (2016) 690–701.
[20] A. Thompson, I. Maskery, R.K. Leach, X-ray computed tomography for additive manufacturing: a review, Meas. Sci. Technol. 29 (2016) 072001(17pp).
[21] N. Kourra, J.M. Warnett, A. Attridge, K. Erchihan, A. Gupta, S. Barnes, M.A. Williams, Metrological study of CFRP drilled holes with X-ray computed tomography, Int. J. Adv. Manuf. Technol. 78 (2015) 2025–2035.
[22] J. Hiller, M. Maisl, L.M. Reindl, Physical characterization and performance evaluation of an X-ray micro-computed tomography system for dimensional metrology applications, Meas. Sci. Technol. 33 (8) (2012) 85404–85422.
[23] G.T. Herman, Fundamentals of Computed Tomography – Image Reconstruction from Projections, Springer, London, 2009.
[24] J. Hsieh, Computed Tomography – Principles, Design, Artifacts, and Recent Advances, 2nd ed., SPIE Press, Washington, USA, 2009.
[25] W. Sun, S.B. Brown, R.K. Leach, An overview of industrial X-ray computed tomography, Queen's Printer and Controller of HMSO, England (2012).
[26] J.P. Kruth, M. Bartscher, S. Carmignato, R. Schmitt, L. De Chiffre, A. Weckenmann, Computed tomography for dimensional metrology, CIRP Ann. Manuf. Technol. 60 (2011) 821–842.
[27] J. Kumar, A. Attridge, P.K.C. Wood, M.A. Williams, Analysis of the effect of cone-beam geometry and test object configuration on the measurement accuracy of a computed tomography scanner used for dimensional measurement, Meas. Sci. Technol. 22 (3) (2011) 35105–35120.
[28] F. Welkenhuyzen, K. Kiekens, M. Pierlet, W. Dewulf, P. Bleys, J.P. Kruth, A. Voet, Industrial computer tomography for dimensional metrology: overview of influence factors and improvement strategies, Proceedings of the 4th International Conference on Optical Measurement Techniques for Structures and Systems: OPTIMESS, Shaker, Antwerp, 2009, pp. 401–410.
[29] W. Dewulf, K. Kiekens, Y. Tan, F. Welkenhuyzen, J.P. Kruth, Uncertainty determination and quantification for dimensional measurements with industrial computed tomography, CIRP Ann. Manuf. Technol. 62 (2013) 535–538.
[30] M. Ferrucci, R. Leach, C. Giusca, S. Carmignato, W. Dewulf, Towards geometrical calibration of X-ray computed tomography systems – a review, Meas. Sci. Technol. 26 (092003) (2015).
[31] N. Otsu, A threshold selection method from gray-level histograms, Automatica (1979) 23–27.
[32] VDI/VDE, Verein Deutscher Ingeniure, 2630 Part1.2: Computed Tomography in Dimensional Measurements, Influencing Variables on Measurement Results and Recommendations for Computed-Tomography Dimensional Measurements, Verein Deutscher Ingeniure, Dusseldorf, 2010.
[33] J.F. Lifton, A.A. Malcolm, J.W. McBride, K.J. Cross, The Application of Voxel Size Correction in X-ray Computed Tomography for Dimensional Metrology, Singapore International NDT Conference & Exhibition, Singapore, 2013, p. 2013.
[34] J.M. Warnett, V. Titarenko, E. Kiraci, A. Attridge, W.R.B. Lionheart, P.J. Withers, M.A. Williams, Towards in-process X-ray CT for dimensional metrology, Meas. Sci. Technol. 27 (3) (2016) 035401.
[35] ISO/NP 10360-11 Geometrical Product Specifications (GPS) – Acceptance and Reverification Tests for Coordinate Measuring Machines (CMM) – Part 11: CMMs Using the Principle of Computed Tomography (CT).
[36] G.T. Herman, Correction for beam hardening in computed tomography, Phys. Med. Biol. 24 (1) (1979) 81.
[37] ISO 3650:1999 Geometrical Product Specifications (GPS), Length Standards, Gauge blocks.
[38] ISO 10360-8:2013 Geometrical Product Specifications (GPS), Acceptance and Reverification Tests for Coordinate Measuring Systems (CMS), CMMs with Optical Distance Sensors.
[39] A. Thompson, L. Korner, N. Senin, S. Lawes, I. Maskery, R. Leach, Measurement of internal surfaces of additively manufactured parts by X-ray computed tomography, 7th Conference on Industrial Computed Tomography, Leuven, Belgium, 2017.